Flux-Weakening Control for IPMSM Employing Model Order Reduction

Mehrnaz Farzam Far, Bilal Mustafa, Floran Martin, Paavo Rasilo, Anouar Belahcen, *Senior Member*, *IEEE*

***Abstract* -- The variation of magnetic parameters due to the magnetic saturation and cross coupling can affect the efficiency and the stability of the control system in electrical machines, especially at high-speed operation. This paper presents an approach independent of the magnetic model parameters to control synchronous motors at the flux-weakening region. In this approach, a model order reduction technique is applied to reduce the finite element model of a synchronous machine. The stator current components and the flux linkage components are the inputs and the outputs of the reduced model, respectively. The reduced model and its inversion are employed to calculate the current reference components from the reference torque. Field oriented control scheme is utilized to implement the overall control system. The proposed control system is validated by means of simulation and experiment on a 2.2 kW permanent magnet synchronous machine.**

***Index Terms*-- Flux weakening, interior permanent magnet synchronous motor, model order reduction, orthogonal interpolation method, vector control.**

I. INTRODUCTION

THE salient feature and low effective air gap of interior permanent magnet synchronous motor (IPMSM) make it well suited for wide speed range operation. Due to overcome of the induced voltage, i.e. back EMF over the maximum available voltage at high speeds, the speed of the machine remains limited [1]. Therefore, flux-weakening control is required to run the machine above a certain base speed.

The control performance of the IPMSM, is deeply influenced if the method applied depends on the machine parameters. Stator resistance and permanent magnet flux linkage are directly affected by temperature changes and cannot retain the fixed values [2]. Furthermore, since the effective air-gap in IPMSM is relatively small, as compared to surface permanent magnet synchronous machine (SPMSM), the armature reaction has a significant effect [3]. This causes magnetic saturation and hence the self-inductances for *d* and *q*-axis (L_d and L_q) vary with the change in the air-gap flux. Cross coupling may also exist between L_d and L_q [4]. This effect becomes significant especially in the flux-weakening region. Notably, the *q*-axis inductance exhibits more variation and depends on the current in that axis, whereas the *d*-axis inductance in comparison remains uniform [5].

Several studies investigating the magnetic cross coupling saturation have been carried out for achieving a more robust control model of electrical machines [6] - [9]. The authors of [6] suggest a flux-observer based control scheme for this purpose. However, according to the authors, this scheme is not applicable when using the stationary frame as the reference. The authors of [7] derive a saturated model by defining a single factor saturation as the ratio between the saturated inductance and the unsaturated one. In [8], a nonlinear state equation is applied to include both the iron loss and the magnetic cross-saturation in the vector control of a synchronous reluctance motor. The nonlinear state equation is obtained from an approximate equation, by measuring the inductances and the iron loss resistance from standstill and no-load rotating tests, respectively. The authors of [9] introduce explicit power functions to include the cross-saturation in a motion-sensorless synchronous reluctance machine.

Reference [10] attempts to reduce the effect of parametric sensitivity based on an analytical approach by using look-up tables. This reference manipulates both feedforward and feed path mechanism and shows that the torque obtained through this approach remains close to the maximum torque available in the flux-weakening region. Some authors suggest usage of on-line and off-line parameter estimation through the usage of optimal look-up tables [11] - [13]. In all these methods, either the error estimation of magnetic parameters or the slight difference in the identified model can lead to the degraded performance. Furthermore, the look-up tables in most of these techniques can be computationally demanding and upsurge the complexity itself.

Virtually, it is possible to compute the magnetic parameters accurately via the finite element (FE) method (FEM), but this requires the knowledge of the machine dimensions and material properties. FEM can solve the electromagnetic system of equations accounting for the nonlinear behavior of the material. Nevertheless, a direct implementation of FE model in a real-time control system is impossible due to the limitation on the computational time. In this paper, we use a model order reduction (MOR) technique on the FE model of an electrical machine to derive a faster and accurate representation of the machine. The reduced model is then applied to control an interior permanent magnet synchronous motor (IPMSM). The dimension and the complexity of the reduced model is significantly lower than that of the FE model

This work has been supported by the Academy of Finland, Helsinki, Finland, under Grant 287395 and Grant 297345 and the Estonian Research Council under grant PUT1260.

M. Farzam Far, B. Mustafa, and F. Martin are with the Department of Electrical Engineering and Automation, Aalto University, FI-02150 Espoo, Finland.

P. Rasilo is with the Laboratory of Electrical Energy Engineering, Tampere University of Technology, P.O. Box 692, FI-33101 Tampere, Finland.

A. Belahcen is with the Department of Electrical Engineering and Automation, Aalto University, FI-02150, Espoo, Finland and Department of Electrical Power Engineering and Mechatronics, Tallinn University of Technology, 19086 Tallinn, Estonia.

and therefore it can be used in a real-time application. The proposed method eliminates the effects of magnetic saturation and is entirely independent of the inductances. For the viability of proposition in a wide range of speed, we provide the results of torque, current, and flux linkage quantities obtained by simulation and experiment. Furthermore, we compare the proposed method with an unsaturated control method in terms of flux trajectory and torque-speed curve. To the best knowledge of authors, in the existing literatures, there is no control algorithm combined with the MOR techniques for the control drive of machines in the flux-weakening region.

In the succeeding section, organization of the paper is as follows. Section II describes briefly the mathematical modelling of an IPMSM and a magnetic model based on MOR. Section III details the feasible operating area of a PMSM, the methodology of the control technique and the implementation of MOR in the algorithm. In Section IV, we provide the simulation and the experimental results of the proposed method applied to a 2.2 kW IPMSM drive. Finally, conclusion is presented in the last section.

II. MODELING OF IPMSM

A. Fundamental Equations

Considering the equivalent circuit of an IPMSM, one can write the stator voltage equation in the (d, q) rotor coordinate frame as:

$$u_{\mathrm{d}} = R_{\mathrm{s}} i_{\mathrm{d}} + \frac{d\psi_{\mathrm{d}}}{dt} - \omega_{\mathrm{r}} \psi_{\mathrm{q}} , \tag{1}$$

$$u_{\mathrm{q}} = R_{\mathrm{s}} i_{\mathrm{q}} + \frac{d\psi_{\mathrm{q}}}{dt} + \omega_{\mathrm{r}} \psi_{\mathrm{d}} . \tag{2}$$

In linear magnetic materials, the flux linkages are given by:

$$\psi_{\mathrm{d}} = L_{\mathrm{d}} i_{\mathrm{d}} + \psi_{\mathrm{pm}} , \psi_{\mathrm{q}} = L_{\mathrm{q}} i_{\mathrm{q}} . \tag{3}$$

The notations used in (1) – (4) are designated as:
u_{d}, u_{q}: d and q-axis voltage components,
i_{d}, i_{q}: d and q-axis current components,
ψ_{d}, ψ_{q}: d and q-axis flux linkage components
R_{s}: Stator resistance,
ω_{r}: Electrical angular velocity,
L_{d}, L_{q}: d and q-axis inductances,
ψ_{pm}: Permanent magnet flux.

The electromagnetic torque T_{e} is computed from the flux linkages, currents, and the number of pole pairs p as follows:

$$\begin{aligned} T_{\mathrm{e}} &= 1.5p(\psi_{\mathrm{d}} i_{\mathrm{q}} - \psi_{\mathrm{q}} i_{\mathrm{d}}) \\ &= 1.5p(\psi_{\mathrm{pm}} i_{\mathrm{q}} + (L_{\mathrm{d}} - L_{\mathrm{q}}) i_{\mathrm{q}} i_{\mathrm{d}}) . \end{aligned} \tag{4}$$

The term $1.5p(L_{\mathrm{d}} - L_{\mathrm{q}})i_{\mathrm{q}}i_{\mathrm{d}}$ in (4) represents the reluctance torque in addition to the already available magnetic torque term $1.5p\psi_{\mathrm{pm}}\, i_{\mathrm{q}}$. It is perceptible that the negative value of i_{d} will be an addition to the torque expression when L_{d} is less than L_{q}.

The magnetic circuit of an actual machine experiences saturation as the magnetic flux increases. In this case, the inductances and the magnetic flux components are functions of the current components. Fig. 1 is an example of the dependency of the stator flux linkages on both components of the stator current from the FE model of the IPMSM under study. Although this machine does not experience high saturation at high currents due to its structure properties, the cross-saturation phenomenon is more vivid on q component of the flux linkage than on the d component.

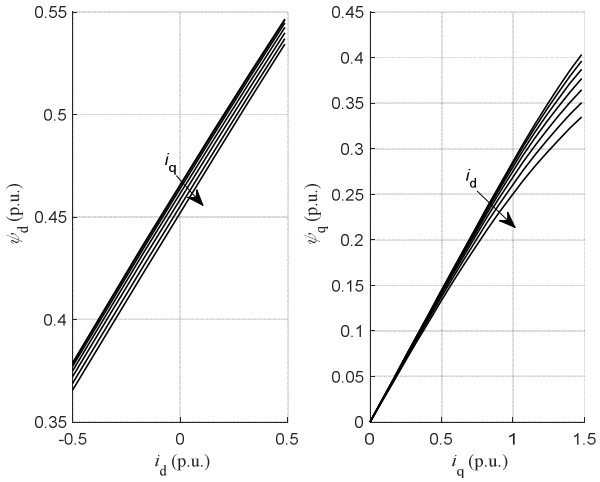

Fig. 1. Computed variation of the flux linkages with respect to the stator current components. The arrows directions show increasing currents.

The FE model considers the magnetic saturation characteristic of the motor in the computation of the stator flux linkage components, without the usage of the inductances. In the next subsection, we propose a reduced model of the FE model, which considers the cross-saturation characteristic of the motor and can be applied in the real-time control.

B. Magnetic Model Based on Orthogonal Interpolation

The FEM is employed to accurately solve the system of equations of electrical machines. The system of equations of an electrical machine with a magnetostatic field is presented in form of:

$$\boldsymbol{S}\boldsymbol{a} = \boldsymbol{F} , \tag{5}$$

where $\boldsymbol{S}$ is the stiffness matrix with size of $m \times m$, with m to be the total number of nodes in the FE mesh. $\boldsymbol{a}$ is a vector of size m containing the nodal values of the magnetic vector potentials, and $\boldsymbol{F}$ is the source vector of size m. In nonlinear material, the stiffness matrix $\boldsymbol{S}$ depends on $\boldsymbol{a}$, which makes the system nonlinear and a Newton-Raphson iteration scheme is often applied in solving (5).

MOR can be used to reduce the complexity, the computational time, and the order of (5), irrespective of its non-linearity. There are different kinds of methods implemented to perform this task that include Lauguerre methods, Arnoldi and PRIMA method, and proper orthogonal decomposition method [14]. The method, however, used in this paper to apply MOR is orthogonal interpolation method (OIM) [15].

Like some other MOR techniques, the set of data to be involved in constructing the OIM based reduced model plays a vital role in the accuracy of the results. The methodology adopted in this technique, to appropriately attain the reduced

model, is the method of snapshots. Snapshots refer to the output data of the system that can be obtained through the experiments or the numerical method, in frequency domain, time domain, or any other configuration. These solutions, nodal values of the magnetic vector potential in our case, are saved in a matrix called snapshot matrix $\boldsymbol{A}_\mathrm{n}$ of size $m \times n$, where n ($n << m$) refers to the number of solutions for the system under study. The snapshot matrix can be decomposed into orthogonal basis by using singular value decomposition (SVD) as:

$$\boldsymbol{A}_\mathrm{n} = \boldsymbol{U}\boldsymbol{\Sigma}\boldsymbol{V}^\mathrm{T} . \tag{6}$$

SVD is a factorization process involving three transformations, first of which is performed by right singular vectors in $\boldsymbol{V}^\mathrm{T}$ followed by the extension along the coordinate axis by $\boldsymbol{\Sigma}$ and the final rotation with the left singular vectors in $\boldsymbol{U}$. $\boldsymbol{U}$ and $\boldsymbol{V}$ are orthogonal matrices of size $m \times m$ and $n \times n$, respectively. $\boldsymbol{\Sigma}$ is a rectangular diagonal matrix with size $m \times n$ and its diagonal entries represent the nonnegative singular values σ_i that are arranged as $\sigma_1 > \sigma_2 > \ldots > 0$. The energy of the matrix is defined as the square sum of the singular values. The first r singular values ($r << n << m$) captures the most energy of the system. Therefore, the first r singular values and the corresponding left and right singular vectors are sufficient to reconstruct the snapshot matrix. In this way, we replace the matrices $\boldsymbol{U}$, $\boldsymbol{\Sigma}$, and $\boldsymbol{V}^\mathrm{T}$ by $\boldsymbol{U}_\mathrm{r}$, $\boldsymbol{\Sigma}_\mathrm{r}$, and $\boldsymbol{V}_\mathrm{r}^\mathrm{T}$ with the size of $m \times r$, $r \times r$, and $r \times n$, respectively.

The main difference between OIM and some other projection-based methods like proper orthogonal decomposition is that we mainly focus on the reduced right singular vectors i.e. columns of $\boldsymbol{V}_\mathrm{r}$ instead of the reduced left singular vectors i.e. columns of $\boldsymbol{U}_\mathrm{r}$. The product of two matrices $\boldsymbol{U}_\mathrm{r}$ and $\boldsymbol{\Sigma}_\mathrm{r}$ remains same for any input variable within the domain of snapshot matrix. However, the columns of $\boldsymbol{V}_\mathrm{r}^\mathrm{T}$ vary depending on the input set f from which the snapshot matrix is built, as expressed in (7). The input set can be time, frequency, voltage, current, rotation angle, etc.

$$\boldsymbol{V}_\mathrm{r}^\mathrm{T} = \begin{pmatrix} v_{11} & \cdots & v_{1n} \\ \vdots & \ddots & \vdots \\ v_{r1} & \cdots & v_{rn} \end{pmatrix} \begin{matrix} \\ \\ \uparrow \\ f_1 \end{matrix} \quad \begin{matrix} \\ \\ \uparrow \\ f_n \end{matrix} . \tag{7}$$

For any new input set within the snapshot range, each components of the new vector $\hat{\boldsymbol{V}}_\mathrm{r}^\mathrm{T} = [\hat{v}_{11} \quad \ldots \quad \hat{v}_{r1}]$ is obtained by interpolating the corresponding right singular vector of $\boldsymbol{V}_\mathrm{r}$. The nodal values of the magnetic vector potential for this new input set can be given as:

$$\hat{\boldsymbol{A}} = \boldsymbol{U}_\mathrm{r}\boldsymbol{\Sigma}_\mathrm{r}\hat{\boldsymbol{V}}_\mathrm{r}^\mathrm{T} . \tag{8}$$

Thereafter, the magnetic flux linkage for each phase winding of the machine can be expressed as an integral of the magnetic vector potential over the whole problem region Ω as:

$$\psi_x = \frac{Nl}{C_\mathrm{T}} \sum_{j=1}^{n} \int_\Omega \beta N_j \mathrm{d}\Omega a_j , \tag{9}$$

here, x represents any one of the phases A, B or C. N and l represent the number of coil turns and the core length of the machine, respectively. C_T is the total cross-section area of the coils in series. β depends on the direction of the coil sides. β is 1 if the nodes are located within the positive coil sides, -1 if the nodes are located within the negative coil sides, and zero elsewhere. N_j and a_j are the FE shape function and the nodal value of the vector potential of node j, respectively. The coefficients of a_j in (9) are constant for a given machine design, therefore, these coefficients are computed once and in advance the flux computation.

III. Control Scheme

A. Feasible Operating Area

The maximum current limit of a motor depends on the inverter current limit and the machine thermal current limits and is represented in the form of:

$$\sqrt{i_\mathrm{d}^2 + i_\mathrm{q}^2} \le I_\mathrm{max} . \tag{10}$$

In the i_d-i_q plane, a circle can be formed of the radius I_max, as shown in Fig. 2. This circle represents the current limit and is independent of the machine speed.

The voltage limit U_max of the inverter depends on the DC link voltage U_dc. In the linear modulation region, this voltage is limited to the range $U_\mathrm{dc}/\sqrt{3}$ [16], which ensures the presence of voltage vector inside the limit. The voltage limit is represented by the set of ellipses. The sizes of these ellipses vary inversely with the angular speed of the machine and the center of these ellipses locate at the point $(-\psi_\mathrm{pm}/L_\mathrm{d}, 0)$ in the i_d-i_q plane, i.e. Fig. 2. The voltage limit equation is:

$$\sqrt{u_\mathrm{d}^2 + u_\mathrm{q}^2} \le U_\mathrm{max} . \tag{11}$$

In the steady sate and by neglecting losses, the equation for the maximum flux linkage in the terms of stator currents is given as:

$$\psi_\mathrm{s} = \sqrt{(\psi_\mathrm{pm} + L_\mathrm{d} i_\mathrm{d})^2 + (L_\mathrm{q} i_\mathrm{q})^2} \le \frac{U_\mathrm{max}}{|\omega_\mathrm{r}|} . \tag{12}$$

Fig. 2 also presents the optimal trajectory of the current vector for the whole speed range of operation for an IPMSM with $I_\mathrm{max} < \psi_\mathrm{pm}/L_\mathrm{d}$. In the low speed range, the operating point follows the maximum torque per ampere (MTPA) line, which is path OA in Fig. 2.

As the machine reaches its base speed ω_b, the voltage touches its ceiling point and it is not possible to increase the voltage further to achieve higher speed. Instead, over the base speed, the machine enters the flux-weakening region as the operating point moves along the AB path. The machine reaches the maximum speed ω_max at point B.

The maximum flux linkage in the flux-weakening region is:

$$\psi_\mathrm{s} = \sqrt{\psi_\mathrm{d}^2 + \psi_\mathrm{q}^2} = \frac{U_\mathrm{max}}{|\omega_\mathrm{r}|} . \tag{13}$$

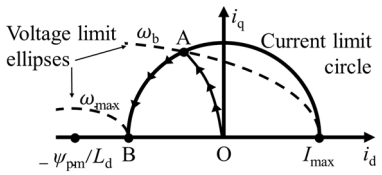

Fig. 2. Optimal trajectory in the i_d-i_q plane for IPMSM.

B. *Control System Based on OIM*

Field oriented control strategy is adopted in the control structure of this paper. Fig. 3 shows the overall control scheme for the machine under study. The rotor position θ_r and the actual speed ω_r of the machine are known by means of an encoder. A proportional-integral (PI) speed controller [17] is used to obtain the torque reference T_{ref}. The current references are generated depending upon the machine speed and the control region. We use a discrete-time current controller [18] to control the current components and attain the reference voltages. Finally, the voltage regulation occurs accordingly to be exerted on motor terminals through space vector pulse width modulation (SVPWM).

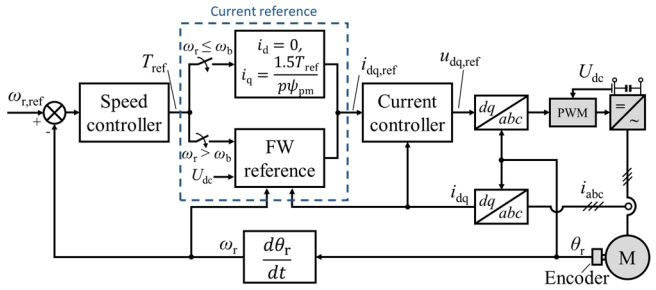

Fig. 3. Proposed block diagram of the control system for an IPMSM. Depending upon the machine speed, current references are computed either via $i_d = 0$ control principle or through the FW reference block.

As mentioned, the computation of the current references depends on the machine speed. If the speed is below the base speed, i.e. the constant torque region, we enforce the *d*-axis current reference $i_{d,ref}$ to be zero and compute the *q*-axis current reference from the torque reference T_{ref} as $i_{q,ref} = 1.5T_{ref} / (p\psi_{pm})$. The $i_d = 0$ control principle is suitable for machines which have low inductances and insignificant armature reaction. Moreover, the implementation of this control method is easy because it maintains a linear relationship between the electromagnetic torque and the *q* component of the current.

When the speed is above the base speed, the flux-weakening region, the control of the machine is no longer possible through the $i_d = 0$ control principle. Instead, a demagnetizing flux is introduced that encounters the fixed flux produced by the permanent magnets. The most feasible means to accomplish this aim is the instigation of negative *d* component of current that fosters the opposing flux. In this case, the magnetic saturation effect cannot be neglected and the variation of L_d and L_q with respect to the current can deteriorate the performance of the system.

To consider the magnetic saturation effect and the coupling between the current components in the flux-weakening region, we propose to implement the OIM in the FW reference block (Fig. 3). The internal structure of the FW reference block is shown in Fig. 4. The conditions to be applied during the control procedures for a region depend on the constraints that need to be followed. For the flux weakening both voltage and current limits need to be considered as mentioned in Section III A.

FW reference block is designed to acquire ψ_d according to the flux-weakening conditions and then generate the current component in the same axis that supports the required flux. The momentarily value of the flux linkage in *q* axis $\psi_{q,est}$ is obtained through the OIM block with the measured current components as input of the block. The construction of the OIM block is explained in the next subsection. The reference *d* component of the flux linkage $\psi_{d,ref}$ is obtained from $\psi_{q,est}$ and (13). It is to be notice that in this region one can compute the magnitude of the flux linkage reference $\psi_{s,ref}$ by the known value of voltage limitation of the inverter U_{dc} and the machine speed as $U_{dc} / (\sqrt{3}\ \omega_r)$.

Subsequently, reference currents are to be produced to proceed towards the current controller. For this purpose, a Simulink feature known as 'algebraic constraint' is availed aptly in conjunction with the OIM block. In the representation of this block, *f(z)* and *z* hint at input and output, respectively. The algebraic constraint block operates in a manner to curb *f(z)* to zero and generates the *z* accordingly. To maintain this sequence of operation, it must have a feedback path that keeps the input at zero. Another key parameter for this block is the 'Initial guess' that will be set according to the required solution value, i.e. 0, to upgrade the solver efficiency.

Here, the error between $\psi_{d,ref}$ and $\psi_{d,OIM}$ behaves as *f(z)*, whereas $i_{d,ref}$ relates with *z* state. A secondary algebraic constraint block is used to provide the input $i_{q,est}$ for the OIM block. The input of this block is the difference between $\psi_{q,est}$, previously obtained from measured i_q, and the *q* component flux $\psi_{q,OIM}$ from OIM block. One can simply compute the *q* component of the current reference $i_{q,ref}$ from (4) by knowing the values of $\psi_{d,ref}$, $\psi_{q,est}$, $i_{d,ref}$, and T_{ref}. However, the value of $i_{q,ref}$ to be passed to the current controller depends on the current limit as well. If the resultant magnitude of $i_{d,ref}$ and $i_{q,ref}$ exceeds the current limit, $i_{q,ref}$ is limited by (10).

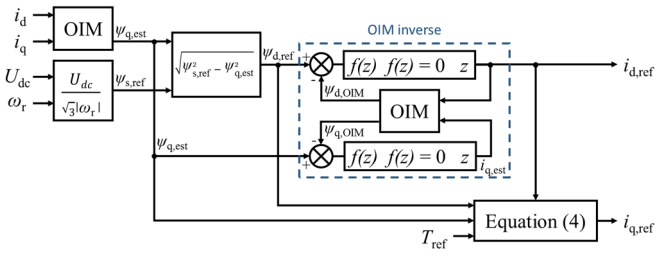

Fig. 4. Internal structure of the FW reference block used in flux-weakening region to calculate current references.

C. *Current-Flux Conversion through OIM*

In this section, we explain the construction of the OIM block from the FE model of the machine under study. The machine is modeled with second-order finite elements with 1379 nodes and electric current supply. The machine parameters are provided in Table I.

As mentioned in Section II B, the first step in building the

reduced model via OIM is to build the snapshot matrix. One of the main factors affecting the accuracy of the reduced model is how the range of i_d and i_q are chosen when generating the snapshot matrix. This range must cover all the possible operating points of the machine. Due to the nature of our control method, i_d is expected to vary from zero to negative rated current and i_q changes from negative rated current to positive rated current. Therefore, the FE model is solved for 40 different operating points of the current components. These operating points are chosen from all the possible combinations of 5 values of i_d, equally distributed in $[-I_N, 0]$, and 8 values of i_q, equally distributed in $[-I_N, I_N]$, with I_N to be the rated current.

The FE results are stored in the snapshot matrix and then decomposed via SVD. The first five singular values capture more than 95 % of the whole energy of the system. The corresponding right singular vectors $[v_1 \dots v_5]$ of these five singular values are selected in constructing the reduced model, by introducing each of the right singular vectors as a function of two variables i_d and i_q. Fig. 5 is an example of the functions for the fourth singular vector versus different values of i_d and i_q.

Thereafter, for any values of the current components, the nodal values of the magnetic vector potential and the flux components are computed using (8) and (9).

TABLE I
PARAMETERS OF THE IPMSM UNDER INVESTIGATION

Parameter	Value
Power	2.2 kW
Winding connection	Star
Rated voltage (rms)	641 V
Rated current (rms)	2.5 A
Rated frequency	75 Hz
Rated speed	1500 r/min
Rated torque	14 Nm
Number of pole pairs	3
Direct-axis inductance	0.108 H
Quadrature-axis inductance	0.159 H
Stator resistance	10.77 Ω
Permanent magnet flux linkage	0.944 Wb
Moment of inertia of rotor and load	0.045 kg·m^2

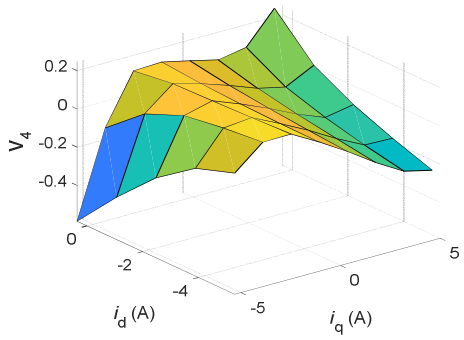

Fig. 5. The fourth right singular vector presented as function of current components i_d and i_q.

IV. RESULTS

The proposed control system is validated by means of simulation and experiment. For the experimental setup, the maximum voltage available at the lab was 370 V. With this voltage, the speed of the machine can rise approximately up to 900 rpm before it enters the flux weakening region. Therefore, due to the voltage limitation, we consider the base speed to be 900 rpm, rather than the rated speed of the machine. The total inertia of the system is also calculated to be 0.045 kgm^2 by performing a deceleration test on the experimental setup.

A. Simulation

The proposed control system is implemented in MATLAB/Simulink environment. Fig. 6 presents the acceleration test for the IPMSM under investigation. The reference speed is changed stepwise from zero to about 1.7 times of the base speed. As it can be seen, the machine enters the flux weakening region at $t \approx 0.7$ s, after which the OIM is used in the reference computation of the current components. It should be noted that the rise time of the speed curve is significantly affected by the total inertia of the system and the high friction acting on the rotor of the PMSM machine.

Fig. 7 illustrates the effect of the magnetic saturation and the cross coupling in the ψ_d-ψ_q plane. The solid curve represents the result from the proposed control system and the dashed curve corresponds to the result when magnetic saturation is not considered. For the latter case, the control system is designed by solely using the rated inductances values. The IPMSM under investigation has low level of saturation and the cross-coupling effect is distinct in ψ_q as i_d increases (this can also be seen in Fig. 1). Therefore, for small values of i_d, both control systems provide similar results. However, as i_d increases in negative direction, the difference between the fluxes is noticeable. Fig. 8 shows the saturation and cross-coupling effects on the torque generation. Based on this figure, the control system without saturation enters the flux weakening region at lower speed and has lower value of torque in this region, compared to the proposed control system.

B. Experiment

For the experimental setup, the IPMSM is coupled with an 11 kW dc motor as the load of the drive system. Fig. 9 provides a picture of the laboratory setup. The Simulink model of the control system is employed in a dSPACE DS1103 PPC board. The experimental results of the control drive are shown in Fig. 10. The speed reference set to same value as in the simulation. The experimental results match with the simulation results, except for the noises in waveforms. These noises are mainly generated from the spatial harmonics of the IPMSM.

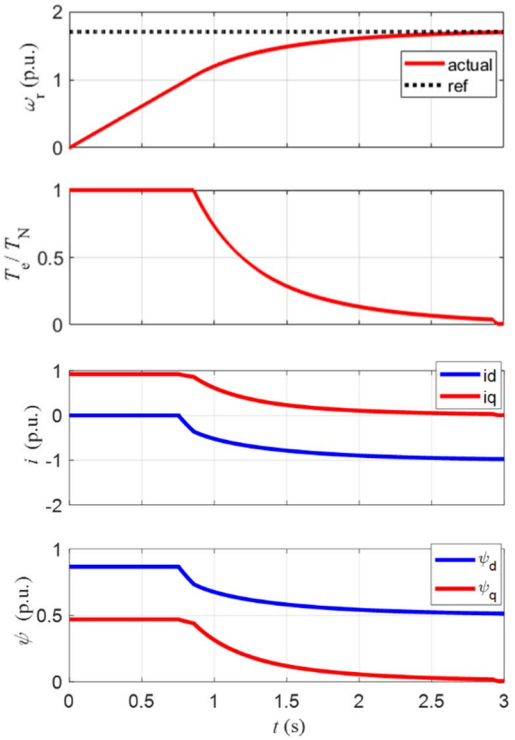

Fig. 6. Simulation results for the 2.2 kW PMSM. Speed reference is set to 1.7 pu. The first subplot shows the reference speed and the actual speed. The second subplot shows the ration of the estimated torque to the rated torque of the machine. The third and the last subplots show the measured current components and the flux components, respectively.

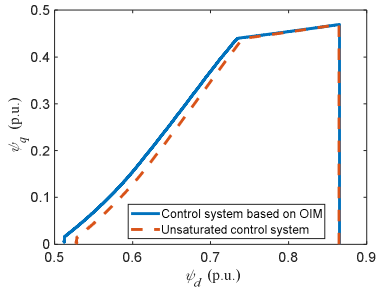

Fig. 7. Control trajectory in the ψ_d-ψ_q plane.

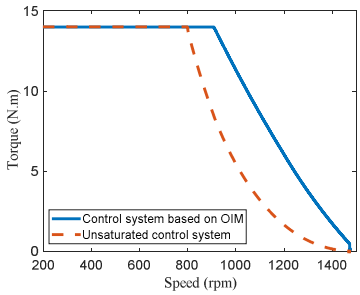

Fig. 8. Torque vs speed curve.

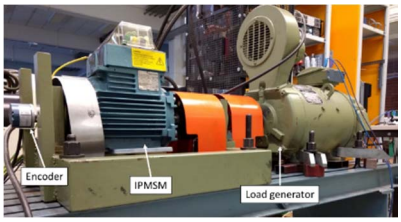

Fig. 9. Picture of the laboratory setup.

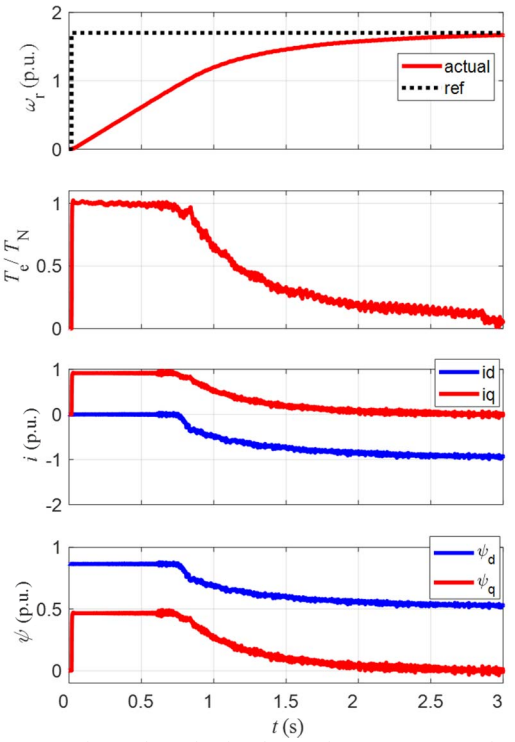

Fig. 10. Experimental results for the 2.2 kW PMSM. Speed reference is stepped from zero to 1.7 pu.

V. Conclusion

In this paper, we propose a novel control method based on a MOR technique, i.e. OIM, that is obtained by reducing the order of the FE model of an IPMSM, effectively. The functionality of an in-built Simulink feature, i.e. 'algebraic constraint', is utilized altogether with the OIM model to generate the current references for the current controller as required in the field-oriented control scheme. The proposed method is implemented in the flux weakening control of an IPMSM, however, the same approach can be applied to any synchronous motors at different operating speed range.

The principal advantage of this method is that it eliminates the effect of magnetic saturation, cross coupling, and parameter sensitivity, since the method is independent of the motor parameters such as L_d, L_q, and the PM flux. Moreover, since the OIM significantly reduces the number of unknowns, it can be an efficient substitute for the look-up tables in the control systems. The simulation and experimental results, provided in the last section of the paper, validate the feasibility of the proposed control method. In the future work, we will consider the spatial harmonics in the model and study the effect of torque loading on the control method.

VI. Acknowledgment

The authors would like to thank Mr. Hafiz Asad Ali Awan for his guidance in the control design.

VII. References

[1] J. F. Fuller, E. F. Fuchs, and K. J. Roesler, "Influence of harmonics on power distribution system protection," *IEEE Trans. Power Delivery*, vol. 3, pp. 549-557, Apr. 1988.

[2] E. H. Miller, "A note on reflector arrays," *IEEE Trans. Antennas Propagat.*, to be published.
[3] R. J. Vidmar. (1992, Aug.). On the use of atmospheric plasmas as electromagnetic reflectors. *IEEE Trans. Plasma Sci.* [Online]. *21(3)*, pp. 876-880.
[4] E. Clarke, *Circuit Analysis of AC Power Systems*, vol. I. New York: Wiley, 1950, p. 81.
[5] G. O. Young, "Synthetic structure of industrial plastics," in *Plastics*, 2nd ed., vol. 3, J. Peters, Ed. New York: McGraw-Hill, 1964, pp. 15-64.
[6] A. Vagati, M. Pastorelli and G. Franceschini, "High-performance control of synchronous reluctance motors," *IEEE Trans. Ind. Appl.*, vol. 33, no. 4, pp. 983-991, Jul/Aug 1997.
[7] T. Lubin, H. Razik, and A. Rezzoug, "Magnetic saturation effects on the control of a synchronous reluctance machine," *IEEE Trans. Energy Convers.*, vol. 17, no. 3, pp. 356–362, Sep. 2002.
[8] S. Yamamoto, T. Ara and K. Matsuse, "A method to calculate transient characteristics of synchronous reluctance motors considering iron loss and cross-magnetic saturation," *IEEE Trans. Ind. Appl.*, vol. 43, no. 1, pp. 47-56, Jan. 2007.
[9] Z. Qu, T. Tuovinen and M. Hinkkanen, "Inclusion of magnetic saturation in dynamic models of synchronous reluctance motors," *2012 XXth Int. Conf. Electric. Mach.*, Marseille, 2012, pp. 994-1000.
[10] T. S. Kwon, G. Y. Choi, M. S. Kwak, and S. K. Sul, "Novel flux weakening control of an IPMSM for quasi-six-step operation," *IEEE Trans. Ind. Appl.*, vol. 44, no. 6, pp. 1722–1731, Nov 2008.
[11] M. Meyer and J. Bocker, "Optimum control for interior permanent magnet synchronous motors (ipmsm) in constant torque and flux weakening range," *2006 12th Int. Power Elect. Motion Cont. Conf.*, Aug 2006, pp. 282–286.
[12] H. A. A. Awan, Z. Song, S. E. Saarakkala, and M. Hinkkanen, "Optimal torque control of synchronous motor drives: Plug-and-play method," *2017 IEEE Energy Convers. Cong. Exposition (ECCE)*, Oct 2017, pp. 334–341.
[13] B. Mansouri and J. Piaton, "Magnetic saturation aids flux-weakening control: using lookup tables based on a static method of identification for nonlinear permanent-magnet synchronous motors," *IEEE Electrification Magazine*, vol. 5, no. 4, pp. 53-61, Dec. 2017.
[14] S. Wilhelmus, A. Henk, V. Vorst, and R. Joost, "Model order reduction: theory, research aspects and applications," Springer-verlag, Berlin, Heilberg, no. 1, p. 2, 2008.
[15] M. Farzam Far, F. Martin, A. Belahcen, L. Montier, and T. Henneron, "Orthogonal interpolation method for order reduction of a synchronous machine model," *IEEE Trans. Magn.*, vol. 54, no. 2, pp. 1–6, Feb 2018.
[16] P. Sarkar and S. Bhunia, "SVPWM based vector control of pmsm drive in delta domain," *2017 Int. Conf. Electr., Comp. Comm. Eng. (ECCE)*, Feb 2017, pp. 5–10.
[17] L. Harnefors, S. E. Saarakkala and M. Hinkkanen, "Speed control of electrical drives using classical control methods," *IEEE Trans. Ind. Appl.*, vol. 49, no. 2, pp. 889-898, March-April 2013.
[18] M. Hinkkanen, H. Asad Ali Awan, Z. Qu, T. Tuovinen and F. Briz, "Current control for synchronous motor drives: direct discrete-time pole-placement design," *IEEE Trans. Ind. Appl.*, vol. 52, no. 2, pp. 1530-1541, March-April 2016.

VIII. BIOGRAPHIES

Mehrnaz Farzam Far received the M.Sc. (Tech.) degree in electrical engineering from Aalto University, Espoo, Finland, in 2014, where she is currently working toward the D.Sc. degree in electrical engineering.

Her research interest includes the numerical modeling of electrical machines.

Bilal Mustafa received the B.Sc. degree in electrical engineering from the University of Engineering and Technology, Lahore, Pakistan, in 2015 and currently working toward the M.Sc.(Tech.) degree at Aalto University.

Floran Martin received his D.Sc. degree from University of Nantes in 2013. He is currently working as a Post-doctoral researcher in Aalto University, department of Electrical Engineering and Automation.

His research is oriented toward magneto-mechanical effects in steel sheets and optimization of electrical machines.

Paavo Rasilo received his M.Sc. (Tech.) and D.Sc. (Tech.) degrees from Helsinki University of Technology (currently Aalto University) and Aalto University, Espoo, Finland in 2008 and 2012, respectively. He is currently working as an Assistant Professor at the Laboratory of Electrical Energy Engineering, Tampere University of Technology, Tampere, Finland.

His research interests deal with numerical modeling of electrical machines as well as power losses and magnetomechanical effects in soft magnetic materials.

Anouar Belahcen (M'13–SM'15) received the M.Sc. (Tech.) and doctors (Tech.) degrees in electrical engineering from the Helsinki University of Technology, Helsinki, Finland, in 1998, and 2004, respectively. He is currently a Professor of electrical machines with the Tallinn University of Technology, Tallinn, Estonia, and Professor of energy and power with Aalto University, Espoo, Finland.

His research interests include numerical modeling of electrical machines, magnetic materials, coupled magnetomechanical problems, magnetic forces, magnetostriction, and fault diagnostics.